INTERNATIONAL JOURNAL OF TECHNO-ENGINEERING
IJTE

ISSN: 2057-5688

THERMAL MAGNETIC CHARACTERISTICS AND CRYSTAL FIELD INTERACTIONS ARE PRESENT IN COMPOSITES

Rachuri Venkataiah, Research Scholar, Department of Physics , Radha Govind University, Ramgarh,Jharkhand.
Dr. Sachin Saxena ,Assistant Professor ,Supervisor, Department of Physics ,Radha Govind University, Ramgarh,Jharkhand.

Abstract: Electrical insulations provide the chance to study the effects on magnetic interaction since they do not include conduction electrons. at the last ten years, studies on various dimerized antiferromagnets that are insulating have found the concave-down phenomena of magnetic susceptibility at magnetic fields that are greater than a particular quantity. It's challenging to comprehend the phenomena. Particular traits of the anomaly lambda's residual heat capacity connected with the superfluid transition in liquid 4He could be seen when the magnetic field rose over the critical threshold. These findings are related to long-range magnetic order, which in the case of indeterminate spin excitations, also known as magnons, is referred to as a Bose Einstein condensation (BEC). Even though magnons are not technically a BEC, it is thought that the BEC description has shown to be quite efficient in explaining some of the values reported of the tiny number of insulating antiferromagnets that display the field-induced concave-down susceptibility at low temperatures. Pb2V3O9, which is given in this BEC description, is one among the systems that displays this concave-down and low temperature sensitivity to magnetic fields owing to a field.

Keywords: Magnetic, Crystal, Composites

I Introduction

INTERNATIONAL JOURNAL OF TECHNO-ENGINEERING
IJTE
ISSN: 2057-5688

Particles with a single domain have a constant magnetization. Domains are divided in nanoparticles over the critical diameter. When thermal fluctuations may arbitrarily alter the direction of a nanoparticle's single domain magnetization, the nano particles are super paramagnetic. The study first examines whether Nano material samples produce thermal energy when exposed to an AC magnetic field. It then compares that to the diameter of particles. Second, it can be determined that the temperature increase around nano particles brought on by the energy released is sufficient to elevate the body temperature of an individual by 68°C. A temperature shift of this magnitude is required for the human body to go from 37°C to around 45°C, which is the temperature at which malignant cells are destroyed. This effort intends to test the hypothesis that iron and cobalt generate more heat than the commonly employed iron oxide.

FERROMAGNETISM

Magnetization occurs spontaneously in ferromagnetic materials. Even in the absence of a magnetic field from the outside, there is magnetization. Anisotropy, or the parallel alignment of a major portion of the molecular magnetic moments in a crystal, is a necessary component of ferromagnetism [1]. All moments are parallel and aligned at absolute zero. Below a threshold temperature Tc, also known as the Curie temperature, which varies depending on the substance, ferromagnetism manifests itself. Materials display permanent magnetism below this temperature because the magnetic moments are highly ordered, but materials above it are paramagnetic because the magnetic moments have a random orientation. The 3d and 4f energy shells that aren't full are connected to ferromagnetism.

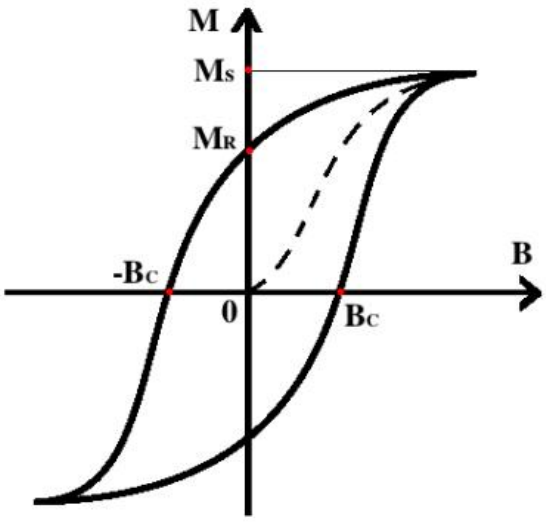

Figure 1: Hysteresis loop.

INTERNATIONAL JOURNAL OF TECHNO-ENGINEERING
IJTE
ISSN: 2057-5688

Ferromagnetic substances gradually grow its magnetic strength under the influence of a magnetic field, starting from to a maximum value, as shown by the dashed line shown in Figure 1, which is the magnetization curve that started[2]. The MS saturation (spontaneous magnetization) is the point at which magnetization reaches its maximum value, initially increases rapidly before slowing before eventually reaching a constant amount. The magnetic field gradually decreases in line with the curve over the initial curve of [3] If the field is declining. The residual magnetization or MR or MR, is the magnetic field when it reaches zero. The field must be applied known as the coercive force field which is also known as C, in opposite directions in order to decrease the magnetic field to zero. The saturation of the magnetization in the opposite direction can result from a subsequent increase in the field of coercivity (coercivity). Loops, also known as a hysteresis-like loop of magnetization, can be closed by repeating the exact event with the reverse direction.

The size of particles decreases, the configuration changes from multi-domain to single-domain because of conflicts between the domain wall energy and the magnetostatic[4]. In the end, particles have an upper limit of size at that point at which the multi domain arrangement cannot be sustained, and also where the building of a wall is more demanding than supporting the magnetic energy of a single, uniformly magnetized domain where all spins are aligned in a single direction. The only method for magnetization in single domain nano particles involves spin rotation. If the EDW of the domain (EDW) as well as the magneto static energy (EMS) are equal, EMS = EDW, the single-domain nano particle's critical diameter (Dc) is attained. The co-ercivity is at its highest at the Dc. This maximum's location is influenced by the material contributions made by various anisotropy energy components. Usually, the Dc is between 10 and 100 nano meters. The critical diameter may be stated as a function of the magnetic properties of the nano particle in the case of a strong anisotropy. Since the numbers in the Table were found

INTERNATIONAL JOURNAL OF TECHNO-ENGINEERING
IJTE
ISSN: 2057-5688

experimentally, there are significant discrepancies between them. Additionally, magnetic characteristics at the nanoscale largely rely on the manufacturing process, shape, size, and The size distribution of the sample. The critical dimension of nanoparticles is important for magnetic materials that exhibit weak anisotropy[5].

II Related Work:

A crystal is a regular collection of atoms or molecules, and the crystal lattice is the pattern in which they are repeated in space. An electron moving through a crystal exhibits a periodic potential, and the crystal's conduction characteristics are determined by both its contents and the geometry of the lattice. Electrons move like waves, and they may pass through a periodic potential without scattering if certain conditions are met[6]. The lattice, however, may also prevent certain waves from propagating. The crystal's energy band structure may have gaps where some energies and certain directions of electron motion are prohibited. In order to create improved semiconductor devices, periodic atomic structures' electronic band structures have been engineered. The photonic crystals are the optical equivalent, where the periodic potential is replaced by a periodic dielectric function and the atoms or molecules are replaced by macroscopic media with various dielectric constants. Photonic crystals are periodic electromagnetic structures with photonic band gaps that prevent light from travelling in certain directions at particular frequencies. To regulate the propagation of light and electro magnetic waves, photonic crystals' bandgap and dispersion relation are crucial. Condensed matter physics is becoming more interested in the topic of controlling the propagation of electromagnetic waves in photonic crystals[7]. It is anticipated that photonic crystals will be a crucial component of innovative electro-optical applications in the future.

Recent years have seen the emergence of magnonics as the nexus between the study of spin dynamics and nanotechnology. Magnonic crystals, which are the magnetic counterpart of photonic crystals, are the foundation of magnonics. Magnonic crystal is an

INTERNATIONAL JOURNAL OF TECHNO-ENGINEERING
IJTE
ISSN: 2057-5688

example of a ferromagnetic media in which the magnetic characteristics fluctuate periodically along a certain direction in space. Magnonic bandgaps, which prevent spin waves from propagating in them, have a similar impact on the spectrum of spin wave excitations in magnonic crystals as they do in photonic crystals[8]. Magnonic crystals, which are ferromagnetic materials with periodic distributions of various materials or particular material properties (such as saturation magnetization or anisotropy), as well as other modulated properties like an external magnetic field that affects the propagation of spin waves, are described in the previous chapter. Magnonic systems can exhibit periodicity in a variety of ways, including (i) material parameter modulation, (ii) surface corrugation (width or thickness modulation), (iii) periodic boundary condition modulation at nonmagnetic medium interfaces, and (iv) application of a periodic external magnetic field. The capability of creating a material with desired dynamic qualities arises from periodic modification of the structure or its material properties. This material may then be further tailored by modifying the structure and the material parameters of its component materials[9].

Significant experimental and theoretical effort has been conducted over the last several decades to realise artificial periodicity and tune spin wave dispersion. Numerous different magnonic crystals have been created thus far. The majority of them are constructed from magnetic materials that are regularly modulated, structurally modulated, etc. One of the first efforts to investigate the propagation of spin waves in periodic magnetic structures. Numerous possible uses for magnonic crystals with frequency bandgaps include microwave filters, switches, current-controlled delay lines, etc. The management of the creation and transmission of information-carrying spin waves in devices built on magnonic crystals may benefit from the bandgap's tunability[10].

III Methodology

The need for high-quality single crystal silicon led to the development of the

INTERNATIONAL JOURNAL OF TECHNO-ENGINEERING
IJTE
ISSN: 2057-5688

floating zone crystal growth (FZCG) technique. Field-effect transistors are made of silicon, which made ultra-pure crystalline silicon exceedingly important once they were invented (Ref. [11]).

Crystal growers attempted to create techniques for crystal growing that enabled one to avoid utilising crucibles in order to overcome the purity issue. According to the patents, H. C. Theuerer created a primitive prelude to contemporary FZCG at Bell Labs in 2016 [12]. The device's design is straightforward. A polycrystalline silicon rod is drawn through the area of concentrated heat very slowly. If the circumstances are favourable, big grain single crystals will form, and as no crucible was used in the procedure, they will be of the utmost purity. Modern crystal growers may produce a broad range of samples using more advanced versions of Theuerer's invention. In Fig. 3.1(a), a cartoon of a contemporary gadget is shown. An optical floating zone furnace, also known as an image furnace, is shown in Fig. 3.1(a). Halogen lamps serve as the machine's heat source. These lights have power ratings ranging from 500 W to 2500 W. Two concave, gold-plated mirrors concentrate the lamp's photons.1 Temperatures as high as 2500 K are applied to a volume of just a few cubic millimetres. One sample is polycrystalline.

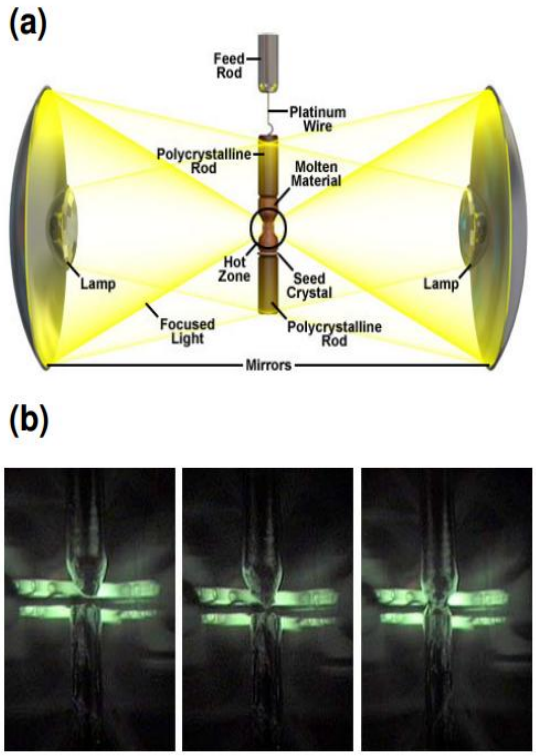

Figure 2 : Cartoon representation of an image furnace in (a). (b) A photo captured by an image furnace camera shows how rods were attached to produce a molten zone. These numbers are from Reference [13].

A rod is suspended from a shaft that moves vertically, and another is

INTERNATIONAL JOURNAL OF TECHNO-ENGINEERING
IJTE
ISSN: 2057-5688

fastened to a collinear shaft that lies below. The lower shaft is likewise mobile. A quartz tube surrounds the sample and shafts. Now that the environment is under check. The rods are programmed to rotate between 5 and 200 revolutions per minute. As shown in Fig. 3.1(b), the sample rod tips are inserted into the hot zone and melted. A video camera is used to monitor the formation process of the molten zone that is brought into contact at the bottom of the top rod and the top of the bottom rod, respectively. Controlling the molten liquid zone is often challenging. Liquid "dropping" happens when there is too much liquid in the area for the surface tension to hold it against gravity. Optimising growth conditions is a never-ending task since little variations in polycrystalline rod diameters or lamp voltages may sometimes result in significant differences in the behaviour of the sample. Because of how enjoyable they are to operate, floating zone furnaces need both art and science to master.

$$p(\vec{\mathbf{r}}) = p(\vec{\mathbf{r}} + \vec{\mathbf{R}}) = \sum_{\vec{\mathbf{x}}} p_{\vec{x}} e^{i\vec{\mathbf{x}}\cdot\vec{\mathbf{r}}} = \sum_{\vec{\mathbf{x}}} p_{\vec{x}} e^{i\vec{\mathbf{x}}\cdot(\vec{\mathbf{r}}+\vec{\mathbf{R}})}$$

$$p_{\vec{x}} = \frac{1}{V}\int p(\vec{\mathbf{r}}) e^{-i\vec{\mathbf{x}}\cdot\vec{\mathbf{r}}} dV.$$

For x R equal to an integer multiple of 2, the Fourier transformations are periodic. The reciprocal lattice vector R = m1a, with m taking on integer values, is the best option for "x."

$$\vec{\mathbf{a}_1^*} = 2\pi \frac{\vec{\mathbf{a}_2} \times \vec{\mathbf{a}_3}}{\vec{\mathbf{a}_1} \cdot (\vec{\mathbf{a}_2} \times \vec{\mathbf{a}_3})}$$
$$\vec{\mathbf{a}_2^*} = 2\pi \frac{\vec{\mathbf{a}_3} \times \vec{\mathbf{a}_1}}{\vec{\mathbf{a}_2} \cdot (\vec{\mathbf{a}_3} \times \vec{\mathbf{a}_1})}$$
$$\vec{\mathbf{a}_3^*} = 2\pi \frac{\vec{\mathbf{a}_1} \times \vec{\mathbf{a}_2}}{\vec{\mathbf{a}_3} \cdot (\vec{\mathbf{a}_1} \times \vec{\mathbf{a}_2})}.$$

The geometry for two plane waves2's XRD scattering is shown in Figure 3.3. Two charges are represented by the blue circles. The wave numbers of incoming and scattered photons, k i and k f, respectively, describe plane waves with wave vectors of the form k = 2/n, where n is a unit vector pointing in the direction of k and is the wavelength of the incident and dispersed photons3

Geometries that reflect light are also feasible. Using a MoK radiation-powered Oxford-Diffraction Xcalibur2 system, the sample's crystallinity was assessed. In order to gather data at 180 K, as-grown samples were cut to the proper size in paratone-N oil and placed in a cryo-loop. Using a

INTERNATIONAL JOURNAL OF TECHNO-ENGINEERING
IJTE
ISSN: 2057-5688

customised 4-circle diff-ractometer with CuK radiation, larger crystals were assessed and orientated. The following chapter contains the results of the improvements.

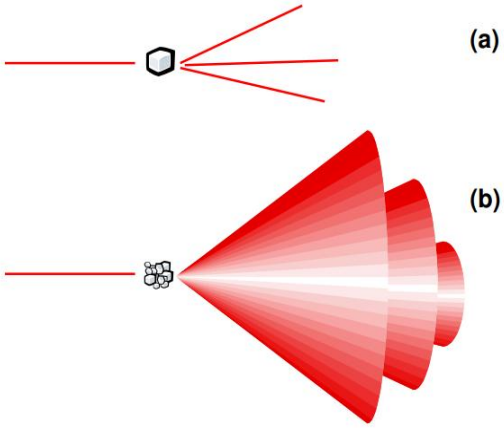

Figure 3: Forward scattering in a sample of one crystal. polycrystalline sample (b).

IV Experiments and Results

In the present experiment, all chemicals are of a high purity analytical grade and are employed without additional purification. In the current study, hematite was synthesised at various pH and calcination temperatures. Following the gradual dissolution of a 2 M ammonia solution in a ferric chloride solution, FeCl3 was first dissolved in 2 M hydrochloric acid to create a solution with a concentration of 1 M for FeCl3. The reaction's pH was maintained at 5, 7, 9, and 11. For two hours, the aqueous solution was agitated to achieve the complete precipitation. The precipitate was filtered, cleaned three times with ethanol and deionized water, and then allowed to dry for 12 hours in the air at 70 ° C. The precursors were then calcined for two hours in air at 400 °C. The precursor (pH 9) was calcined at several temperatures—300, 500, and 600 °C—for two hours in air to examine the impact of calcination temperatures. After the heat treatment, the colour of the precursor product changed from brown to deep red. By precipitating Fe3+ and Fe2+ ions in a 2:1 molar ratio in the presence of ammonia as a base solution, Fe3O4 nanocrystals were created. The chemical reaction recorded in

Thus, 2M FeCl3 and 1M FeCl24H2O were dissolved in a 2M hydrochloric acid solution. This solution was then gradually added to with 2M ammonia until the pH ranged from 5 to 11. For an extra hour, the reaction was stirred. The black precipitate was filtered, washed three times with ethanol and

INTERNATIONAL JOURNAL OF TECHNO-ENGINEERING
IJTE
ISSN: 2057-5688

deionized water, and then dried at 70 °C for 12 hours in a vacuum, much like the prior procedure. The pH 9 sample was chosen for the second stage, which included heating it for two hours in air at temperatures between 150 and 450°C.The product's hue was altered to brown throughout the heating process for the black. By scanning at a step rate of 0.02 per minute and using Cu K radiation with a wavelength of 1.5406 over the angular range of 10-80, the crystalline structure of the as-prepared samples was identified. The morphology was studied using a transmission electron microscope (TEM, JEOL JEM-2100F 200kV) and field emission scanning electron microscopy (FE-SEM, MERLIN-ZEISS).A vibrating sample magnetometer (VSM, Lake Shore 7407) was used to test the magnetic characteristics of the material at room temperature. Using a UV-VIS-NIR light spectrophotometer (JASCO, V570) in transmission mode, the optical characteristics of the nanocrystals were examined.

The pH 5 to 11 samples were produced after being calcined at 400 °C, and their XRD patterns are shown in Fig. 3.1. By contrasting them with JCPDS No. 33-0644, the peaks were located. The one phase of -Fe2O3 was identified by the XRD patterns. As-prepared -Fe2O3 nanoparticles crystallised with a rhombohedral lattice structure (space group: R3c) in the hexagonal crystal system [14]. No further crystalline phases or impurities were found in the samples according to the XRD data. The strength of the peaks diminished as pH climbed.

Where is the full width at half maximum (FWHM) of the diffraction peak, is the diffraction angle, and is the radiation wavelength. The crystallite size was determined using the (1 0 4) plane. Table 3.1 shows the relationship between the average crystalline sizes of -Fe2O3 and pH. According to the data, higher pH causes a reduction in crystalline size. The pH of the solution continued to rise as the base solution was added, and the size of the particles shrank. Precipitate dissolves when the pH is high because there are many hydroxyl ions (OH-) present. Additionally, Vayssieres et al. had seen a decline in mean size when pH was raised [14].

INTERNATIONAL JOURNAL OF TECHNO-ENGINEERING
IJTE
ISSN: 2057-5688

Table 1 shows how the size of -Fe2O3 nanocrystals varies with pH.

pH	FWHM (B)	Crystallite size D, (nm)	Grain size (nm)
5	0.38	22.8	20.5
7	0.44	19.7	30.6
9	0.51	17.0	50.4
11	0.60	14.4	70.8

Fig. 4 shows the powder XRD pattern of the -Fe2O3 samples (pH 9) that were calcined at various temperatures (300 to 600 °C) in the air. The sample's amorphous makeup prevents peaks from appearing in the XRD pattern at pH 9 (without heating). No further crystalline phases or impurities were found in any of the samples, and the XRD patterns were likewise indexed to the single phase of -Fe2O3. But as the calcination temperature has increased, the diffraction peaks have become stronger and more severe. Table 3.2 lists the relationship between the average Fe2O3 crystallite size and the calcination temperature. According to the data, the crystalline size becomes larger as the calcination temperature rises [8, 9].

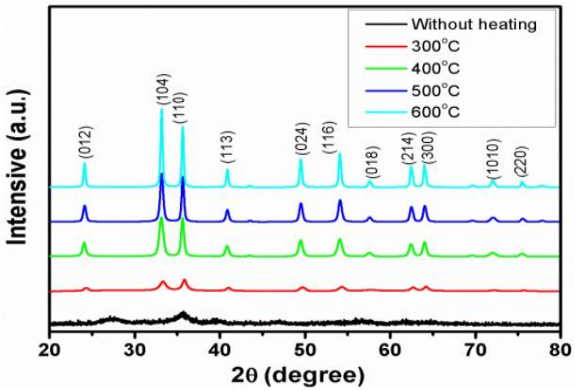

Figure 6 shows the XRD pattern of a nanocrystalline -Fe2O3 for various calcination temperatures.

Table 2 Variation of crystallite size of α-Fe2O3 nanocrystal with different calcination temperatures

T, (°C)	FWHM (B)	Crystallite size D, (nm)	Grain size (nm)
300	1.02	8.5	35
400	0.51	17.0	41
500	0.42	20.6	45
600	0.26	33.3	65

the pH range of 5 to 11 on Fe3O4 nanocrystals' XRD patterns. With the exception of the pH 5 sample, all peaks were indexed in the spinel structure at pH 5, which is due to the by-products such -FeOOH [15]. The XRD pattern reveals that the pH 5 sample has a few additional peaks of -FeOOH. In

INTERNATIONAL JOURNAL OF TECHNO-ENGINEERING
IJTE
ISSN: 2057-5688

addition, the peak intensity is lower in this sample than in other samples because the magnetite structure cannot completely develop. Different pH samples' XRD patterns show line broadenings that seem to be caused by tiny particle sizes.

V Conclusion

Although theoretical techniques and experimental tools are useful for grasping the fundamentals of spin dynamics and obtaining fresh insights into them, there are also some drawbacks to the instruments, such as their mathematical complexity and technological challenges when conducting experiments. In its place, micromagnetic simulations have lately become a potent instrument for the investigation of a wide range of phenomena connected to the spin dynamics of magnetic components on the nanoscale. One kind of numerical experiment used to determine the magnon band structure of a magnonic crystal is micromagnetic simulation. It works well and is often used in the research on the dynamics of magnetization in nanopatterned magnetic systems. The approach is based on numerically solving the whole Landau-Lifshitz equation in real space and time using the finite difference technique or the finite element method. Since studies of magnetization dynamics are difficult and time-consuming, proper simulation process design is crucial.

VI References

(1) Kim, J.-Y.; Kim, E.-R.; Han, Y.-K.; Nam, K.-H.; Ihm, D.-W. Highly Transparent Tin Oxide Films Prepared by DC Magnetron Sputtering and Its Liquid Crystal Display Application. Jap. J. Appl. Phys. 2002, 41, 237.

(2) Comini, E.; Faglia, G.; Sberveglieri, G.; Pan, Z.; Wang, Z. L. Stable and highly sensitive gas sensors based on semiconducting oxide nanobelts. Appl. Phys. Lett. 2002, 81, 1869– 1871.

(3) Snaith, H. J.; Ducati, C. SnO2-Based Dye-Sensitized Hybrid Solar Cells Exhibiting 18 Near Unity Absorbed Photon-to-Electron Conversion Efficiency. Nano Letters 2010, 10, 1259–1265.

(4) Ogale, S. B.; Choudhary, R. J.; Buban, J. P.; Lofland, S. E.; Shinde, S. R.; Kale, S. N.; Kulkarni, V. N.; Higgins, J.; Lanci, C.; Simpson, J. R.; Browning, N. D.; Das Sarma, S.;Drew,

INTERNATIONAL JOURNAL OF TECHNO-ENGINEERING
IJTE
ISSN: 2057-5688

H. D.; Greene, R. L.; Venkatesan, T. High Temperature Ferromagnetism with a
Giant Magnetic Moment in Transparent Co-doped SnO2−δ. Phys. Rev. Lett. 2003, 91, 077205.

(5) Lussier, A.; Dvorak, J.; Idzerda, Y. U.; Ogale, S. B.; Shinde, S. R.; Choudary, R. J.; Venkatesan, T. Comparative x-ray absorption spectroscopy study of Co-doped SnO2 and TiO2. Journal of Applied Physics 2004, 95, 7190–7191.

(6) Hays, J.; Punnoose, A.; Baldner, R.; Engelhard, M. H.; Peloquin, J.; Reddy, K. M. Relationship between the structural and magnetic properties of Co-doped SnO2 nanoparticles. Phys. Rev. B 2005, 72, 075203.

(7) Fitzgerald, C. B.; Venkatesan, M.; Dorneles, L. S.; Gunning, R.; Stamenov, P.; Coey, J. M. D.; Stampe, P. A.; Kennedy, R. J.; Moreira, E. C.; Sias, U. S. Magnetism in dilutemagnetic oxide thin films based on SnO2. Phys. Rev. B 2006, 74, 115307.

(8) Liu, X. F.; Sun, Y.; Yu, R. H. Role of oxygen vacancies in tuning magnetic propertiesof Co-doped SnO2 insulating films. Journal of Applied Physics 2007, 101, 123907.

(9) Zhang, J.; Skomski, R.; Yue, L. P.; Lu, Y. F.; Sellmyer, D. J. Structure and magnetism of V-doped SnO 2 thin films: effect of the substrate. Journal of Physics: Condensed Matter 2007, 19, 256204.

(10) Yu, W.; Jiang, K.; Wu, J.; Gan, J.; Zhu, M.; Hu, Z.; Chu, J. Electronic structures and excitonic transitions in nanocrystalline iron-doped tin dioxide diluted magnetic semiconductor films: an optical spectroscopic study. Phys. Chem. Chem. Phys. 2011,13, 6211–6222.

(11) Li, P.; wen Zhang, C.; Lian, J.; Gao, S.; Wang, X. First-principles study on electronic and magnetic properties of Cu-doped CdS. Solid State Commun. 2011, 151, 1712 – 1715.

(12) Lamrani, A. F.; Belaiche, M.; Benyoussef, A.; Kenz, E. Electronic structures and ferromagnetism of SnO2 (rutile) doped with double-impurities: First-principles calculations. J. Appl. Phys. 2014, 115, 013910.

(13) Inpasalini, M. S.; Choubey, R. K.; Mukherjee, S. Evidence of Bound Magnetic PolaronMediated Weak

INTERNATIONAL JOURNAL OF TECHNO-ENGINEERING
IJTE
ISSN: 2057-5688

Ferromagnetism in co-doped SnO2 Nanocrystals: Microstructural, Optical, Hyperfine, and Magnetic Investigations. J. Electron. Mater. 2016, 45, 3562–3569.

(14) Punnoose, A.; Hays, J.; Thurber, A.; Engelhard, M. H.; Kukkadapu, R. K.; Wang, C.; Shutthanandan, V.; Thevuthasan, S. Development of high-temperature ferromagnetism in SnO2 and paramagnetism in SnO by Fe doping. Phys. Rev. B 2005, 72, 054402.

(15) Wang, H.; Yan, Y.; Mohammed, Y.; Du, X.; Li, K.; Jin, H. First-principle study of magnetism in Co-doped SnO2. J. Magn. Magn. Mater. 2009, 321, 337 – 342.

(16) Coey, J.; Venkatesan, M.; Fitzgerald, C. Donor impurity band exchange in dilute ferromagnetic oxides. Nat. Mater. 2005, 4, 173.

(17) Chang, G. S.; Forrest, J.; Kurmaev, E. Z.; Morozovska, A. N.; Glinchuk, M. D.;McLeod, J. A.; Moewes, A.; Surkova, T. P.; Hong, N. H. Oxygen-vacancy-induced ferromagnetism in undoped SnO2 thin films. Phys. Rev. B 2012, 85, 165319.

(18) Haverkort, M. W. Quanty for core level spectroscopy - excitons, resonances and band excitations in time and frequency domain. J. Phys.: Conf. Ser. 2016, 712, 012001.

(19) Green, R. J.; Boukhvalov, D. W.; Kurmaev, E. Z.; Finkelstein, L. D.; Ho, H. W.; Ruan, K. B.; Wang, L.; Moewes, A. Room-temperature ferromagnetism via unpaired 20 dopant electrons and p − p coupling in carbon-doped In2O3: Experiment and theory. Phys. Rev. B 2012, 86, 115212.

(20) Haverkort, M. W.; Sangiovanni, G.; Hansmann, P.; Toschi, A.; Lu, Y.; Macke, S. Bands, resonances, edge singularities and excitons in core level spectroscopy investigated within the dynamical mean-field theory. Eur. Phys. Lett. 2014, 108, 57004.

(21) Viswanatha, R.; Sapra, S.; Sen Gupta, S.; Satpati, B.; Satyam, P. V.; Dev, B. N.; Sarma, D. D. Synthesis and Characterization of Mn-Doped ZnO Nanocrystals. J. Phys. Chem. B 2004, 108, 6303–6310.